A Fast Image Dehazing Algorithm Using Morphological Reconstruction

Sebastian Salazar-Colores, Eduardo Cabal-Yepez, *Member, IEEE*, Juan M. Ramos-Arreguin, *Senior Member, IEEE*, Guillermo Botella, Luis M. Ledesma-Carrillo, *Student Member, IEEE*, and Sergio Ledesma, *Member, IEEE*

***Abstract*— Outdoor images are used in a vast number of applications, such as surveillance, remote sensing, and autonomous navigation. The greatest issue with these types of images is the effect of environmental pollution: haze, smog, and fog originating from suspended particles in the air, such as dust, carbon, and water drops, which cause degradation to the image. The elimination of this type of degradation is essential for the input of computer vision systems. Most of the state-of-the-art research in dehazing algorithms is focused on improving the estimation of transmission maps, which are also known as depth maps. The transmission maps are relevant because they have a direct relation to the quality of the image restoration. In this paper, a novel restoration algorithm is proposed using a single image to reduce the environmental pollution effects, and it is based on the dark channel prior and the use of morphological reconstruction for fast computing of transmission maps. The obtained experimental results are evaluated and compared qualitatively and quantitatively with other dehazing algorithms using the metrics of the peak signal-to-noise ratio and structural similarity index; based on these metrics, it is found that the proposed algorithm has improved performance compared with recently introduced approaches.**

***Index Terms*— Single-image dehazing, image enhancement, morphological operations, dark channel prior.**

I. Introduction

OUTDOOR images are exposed to adverse weather conditions such as haze, fog or smog, which cause effects such as scene darkening, contrast degradation, and color change, among others. Haze is among the most common atmospheric conditions and is caused by floating particles such as water drops or any other aerosol that reflects the light, diffusing it in the air and reducing the visibility of details. Vision systems applied to remote sensing, surveillance, and autonomous navigation generally use input images under adverse weather conditions; therefore, the results produced depend on the quality of the image received as input. Atmospheric scattering adds nonlinear and data-dependent noise to the captured outdoor image, which makes image restoration a very difficult process; consequently, several research works have focused on diminishing the haze effects in images captured using vision systems by designing and applying dehazing algorithms [1], which can be divided into those requiring additional information from the scene (for instance, in [2], a method for haze removal that utilizes the correlations between hazy images and haze-free images as external information is presented) and those using one single image (in [3], a study and evaluation of existing single-image dehazing algorithms, using a large-scale benchmark of synthetic and real-world hazy images, is presented). The algorithms that use a single image to diminish the effects of adverse atmospheric conditions are the most studied these days because they are useful for practical applications, such as autonomous vehicle navigation, surveillance and remote sensing [4], [5]. In this regard, dark channel prior (DCP), which consists of estimating the transmission map of an image by estimating the depth of each element in it, has been used in combination with other algorithms for fast computation of accurate transmission maps [6], at the cost of long computation times compromising its utilization on online vision systems. Therefore, recent research has focused on the computation speed of transmission maps, aiming to preserve the image quality.

In this work, a novel fast algorithm is proposed for lessening haze effects using morphological reconstruction to preserve important structures in all its stages and refine the transmission-map computation of single images captured by vision systems, making it feasible for use in online applications.

The remainder of the manuscript is organized as follows. Section II provides a brief literature review of related work. Section III introduces an overview of the theoretical background utilized in this work. Section IV describes the proposed technique and its implementation in depth. Obtained results are

Manuscript received February 11, 2018; revised July 20, 2018, September 1, 2018, and October 15, 2018; accepted November 23, 2018. Date of publication December 7, 2018; date of current version January 30, 2019. This work was supported in part by the National Council on Science and Technology (CONACYT), Mexico, under Scholarship 285651, and by DAIP - U. de Gto. under Research Project 209, Convocatoria Institucional de Investigacion Cientifica 2018. The associate editor coordinating the review of this manuscript and approving it for publication was Prof. Khan M. Iftekharuddin. *(Corresponding author: Eduardo Cabal-Yepez.)*

S. Salazar-Colores and J. M. Ramos-Arreguin are with the Faculty of Informatics, Universidad Autónoma de Querétaro, Queretaro 76230, Mexico (e-mail: s.salazarcolores@gmail.com; jramos@mecamex.net).

E. Cabal-Yepez, L. M. Ledesma-Carrillo, and S. Ledesma are with the Division de Ingenierias del Campus Irapuato-Salamanca, Universidad de Guanajuato, Guanajuato 38944, Mexico (e-mail: e.cabalyepez@gmail.com; l.m.ledesmacarrillo@gmail.com; selo@ugto.mx).

G. Botella is with the Departamento de Arquitectura de Computadores y Automatica, Universidad Complutense de Madrid, 28040 Madrid, Spain (e-mail: gbotella@fdi.ucm.es).

Digital Object Identifier 10.1109/TIP.2018.2885490

presented in Section V and compared against those obtained from six different dehazing algorithms. Finally, conclusions are given in Section VI.

II. Related Work

As described before, dehazing algorithms can be divided into two groups. Among those requiring additional information are the following. In [7], a dehazing method is proposed using a visible image with a near-infrared image of the same scene to obtain a dehazed color image. In [8], a system for browsing, enhancing, and manipulating casual outdoor photographs is introduced by combining them with preexisting georeferenced digital terrain and urban models. Other works estimate the captured-scene depth utilizing multiple images taken under different weather conditions [9], [10]. Some algorithms remove haze by taking advantage of light polarization [11], [12]. However, their main disadvantage is that the requirements are not always available or are difficult to comply with. For example, the infrared algorithm requires a modified camera to get the infrared data. It is worth mentioning that algorithms requiring multiple images are difficult to implement for online applications [9], whereas algorithms that use images with different levels of polarization are sensitive to vibrations or movement [10].

Algorithms using a single image to diminish haze effects are among the most relevant research. In [13], haze is removed by maximizing local contrast in the analyzed image. It was noticed that a haze-free image should have higher contrast than a hazed image. In [14], independent component analysis (ICA) is used to address haze by estimating the albedo in the captured scene and the propagation medium, whereas transmission and shading of the surface are correlated locally. In [15], a transmission map is obtained by analyzing the optical model and recasting the initial transmission map under an additional boundary prior. In [16], DCP is proposed for estimating the image transmission map, which consists of estimating each element's depth in the image, and it is essential for restoring it. The presented results are satisfactory; nonetheless, the transmission map generates halos around the restored-image edges. To improve their algorithm, the authors introduced soft matting for polishing the transmission map, sacrificing computation time and jeopardizing its utilization in fast image processing systems for online applications. Consequently, DCP has been used in combination with other algorithms, looking for fast computation of accurate transmission maps [6]. For example, in [17], atmospheric scattering and DCP theories are used for single-image dehazing. A transmission map is estimated using a fast average filter, the region-projection method is adopted to obtain the atmospheric light, and image color compensation is implemented using the Weber-Fechner Law. In [18], a median filter is included for removing halos from an image. In [19], a bilateral filter and a transmission filter are used for removing noise while preserving the edges, and the transmission map is refined to recover the scene. In [20], a correction of white balance is introduced in DCP to improve the image quality by obtaining two components: the reflected light in the image and the light from the environment.

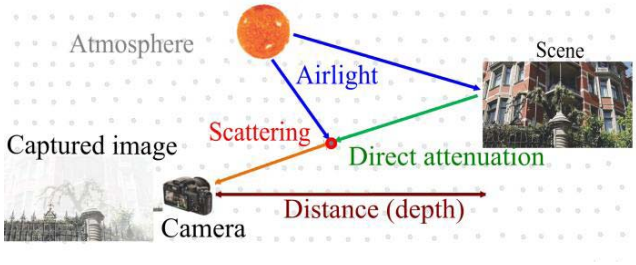

Fig. 1. Atmospheric scattering model.

In [21], a segmentation algorithm called mean shift filtering is proposed for refining the transmission map generated by DCP to improve the reconstructed image. In [22], a fusion-based transmission estimation is introduced, combining the fusion weighting scheme and the atmospheric light computed from the Gaussian-based dark channel method. In [23], a linear color-attenuation prior is proposed based on the difference between the pixel brightness and saturation in hazy images. In [24], a pixel-based algorithm relying on a nonlocal prior and the assumption that a haze-free image can be faithfully represented with just a few hundred distinct colors is proposed.

From the reviewed work in recent literature, it is clear that present research on diminishing haze effects in images focuses on improving the speed of transmission map computation for the original DCP technique [16], [25], without losing the image quality [15]; however, these algorithms have only achieved partial improvements [1], [5]. The contribution of this work is a novel fast algorithm for reducing haze effects, using morphological reconstruction in all its stages to refine the transmission map computation of single images captured by a vision system, making it feasible for online applications. The proposed method is based on the DCP technique and to the best of the authors' knowledge, the introduced approach, which drastically reduces processing time, has never been used for this purpose. In this regard, the technique proposed in this paper is at least two orders of magnitude faster than the original DCP algorithm. Furthermore, obtained qualitative and quantitative results using the Peak Signal-to-Noise Ratio (PSNR) and the Structural Similarity (SSIM) index show that the proposed method achieves better results than other recently introduced state-of-the-art algorithms for this subject.

III. Background

In this section, concepts such as atmospheric scattering, DCP and morphological reconstruction are presented as the framework of the proposed technique for diminishing haze in an image.

A. Atmospheric Scattering Model

Fig. 1 depicts how a scene might be affected by environmental pollution producing haze in the captured image. Its corresponding mathematical model is described by (1) [26].

$$I(\chi) = J(\chi)t(\chi) + A\,(1 - t(\chi)) \tag{1}$$

In (1), $I(\chi)$ is the observed intensity in each channel, R, G and B (RGB), of the pixel $\chi = (x, y)$ in the captured scene

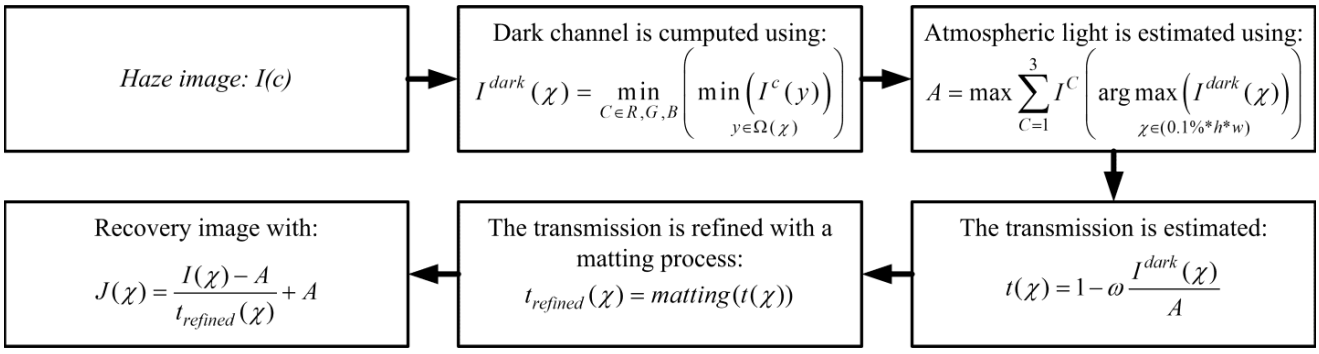

Fig. 2. Dehazing algorithm proposed in [16].

by a camera. $J(\chi)$ is the vector intensity of the scene's original area in the real world that corresponds to the pixel $\chi = (x, y)$. A is the color vector of the global atmospheric light. $t(\chi)$ is called the transmission, which describes the portion of light that is not scattered or absorbed and reaches the camera. Under a homogeneous atmospheric condition, the transmission $t(\chi)$ can be expressed by (2).

$$t(\chi) = e^{-\beta d(\chi)} \tag{2}$$

where β is the atmosphere scattering coefficient and $d(\chi)$ is the depth of the element χ; therefore, a map of transmission is proportional to a depth map. The main difficulty in obtaining $J(\chi)$ rests upon the fact that, when an image is captured, A and $t(\chi)$ in (1) are unknown. Therefore, the use of priors and some assumptions are necessary to find an approximation of $J(\chi)$. The original algorithm, which is based on DCP and was proposed in [16], makes it possible to conduct an accurate estimation of A and $t(\chi)$, but at a high computational cost. Hence, it is necessary to look for an alternative technique able to provide satisfactory results with less processing time.

B. Dark Channel Prior (DCP)

DCP is a statistical observation of what happens in images that do not present the problem of haze and are acquired in external environments. For most of the patches in an image that do not represent the sky, there is at least a low-intensity pixel in each color channel (R, G or B). Thus, the minimal intensity of one pixel in such patches has a value near 0 [16].

For an image $I(\chi)$, the dark channel $I^{dark}(\chi)$ is defined by (3) [16].

$$I^{dark}(\chi) = \min_{C \in R,G,B} \left(\min_{y \in \Omega(\chi)} \left(I^c(y) \right) \right) \tag{3}$$

where $\Omega(\chi)$ is the patch centered in χ, I^C is the color channel C (i.e., R, G, or B) from I, and y is the pixel contained in $\Omega(\chi)$.

Hence, DCP is expressed by (4).

$$I^{dark}(\chi) \to 0 \tag{4}$$

In [16], the algorithm shown in Fig. 2 is proposed to dehaze an image I, of height h and width w pixels, using DCP. The algorithm produces excellent results, but its main drawback is its computational complexity; therefore, in this work, a methodology to dehaze an image is proposed by combining DCP with morphological reconstruction to improve the computation speed for the transmission map estimation of an image.

C. Morphological Reconstruction

The morphological reconstruction is based on mathematical morphology operations, and it is used to simplify images and preserve main features as object shapes. The proposed algorithm uses the concepts of opening and closing for image reconstruction, which are based on techniques such as grayscale erosion, grayscale dilation, geodesic erosion and dilation, and reconstruction by erosion and dilation, considering a grayscale image I, a flat structuring element S with an arbitrary shape formed by pixels s, and the position (x, y) of the pixel χ in the image I.

D. Grayscale Erosion

The erosion ε_B of I by S is defined as the minimum value of the image in the matching region with s when the source is focused at the position $\chi = (x, y)$ [27], as described in (5)

$$[\varepsilon_B(I)](\chi) = \min_{s \in S} I(\chi + s) \tag{5}$$

E. Grayscale Dilation

The dilation δ_B of I by S is defined as the maximum value of the image in the window defined by the origin of S when S is at $\chi = (x, y)$, and it is expressed by (6)

$$[\delta_B(I)](\chi) = \max_{s \in S} I(\chi + s) \tag{6}$$

F. Morphological Reconstruction

A morphological reconstruction is expressed in terms of geodesic dilation and geodesic erosion.

G. Geodesic Dilation

In grayscale images, the size-1 geodesic dilation $\delta_g^{(1)}$ of I (marker image) with respect to F (mask image) is defined by

$$\delta_g^{(1)}(I) = \delta^{(1)}(I) \wedge F \tag{7}$$

where I and F are the same size, the intensity relation $I \leq F$ holds for all pixels in the images, and $\wedge$ is the operator

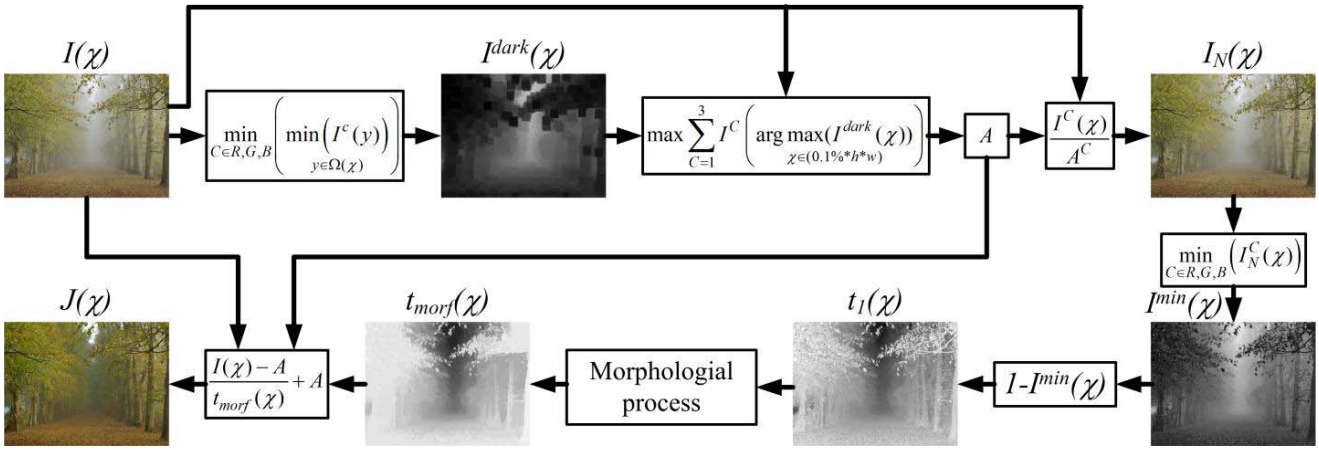

Fig. 3. Flowchart of the proposed algorithm.

minimum. Hence, the n-size geodesic dilation $\delta_g^{(n)}$ is as given in (8).

$$\delta_g^{(n)}(I) = \delta_g^{(1)}[\delta_g^{(n-1)}(I)] \tag{8}$$

with $\delta_G^{(0)}(I) = I$.

H. Geodesic Erosion

In grayscale images, the size-1 geodesic erosion $\varepsilon_g^{(1)}$ of I (marker image) with respect to G (the mask image) is defined by

$$\varepsilon_g^{(1)}(I) = \varepsilon^{(1)}(I) \vee G \tag{9}$$

where I and F are the same size, the intensity relation $I \geq F$ holds for all pixels in the images, and $\vee$ is the operator maximum. The n-size geodesic erosion $\varepsilon_g^{(n)}$ is shown in (10)

$$\varepsilon_g^{(n)}(I) = \varepsilon_g^{(1)}[\varepsilon_g^{(n-1)}(I)], \quad \text{where } \varepsilon_g^{(0)}(I) = I. \tag{10}$$

I. Reconstruction by Dilation

Reconstruction by dilation is obtained through the geodesic dilation of marker I on the mask F, iterating until stability is reached, and it is denoted by $R_g^{\delta}(I)$ as shown in (11).

$$R_g^{\delta}(I) = R_g^{(i)}(I) \tag{11}$$

Stability is reached when $\delta_g^{(i)}(I) = \delta_g^{(i+1)}(I)$.

J. Reconstruction by Erosion

Reconstruction by erosion is obtained through the geodesic erosion of marker I on the mask G, iterating until stability is reached. It is denoted by R_g^{ε} as shown in (12).

$$R_g^{\varepsilon}(I) = \varepsilon_g^{(i)}(I) \tag{12}$$

Stability is achieved when $\varepsilon_g^{(i)}(I) = \varepsilon_g^{(i+1)}(I)$.

K. Opening and Closing by Reconstruction

Opening and closing by reconstruction restore the forms of objects that the structuring element exceeds after each process. The reconstruction precision depends on the similarity of the structuring element to the shape of the objects. The n-size opening by reconstruction of an image I is described by (13). Analogously, closing by reconstruction is defined in equation (14).

$$\gamma_R^{(n)}(I) = R_I^{\delta}[\varepsilon^{(n)}(I)] \tag{13}$$

$$\phi_R^{(n)}(I) = R_I^{\varepsilon}[\delta^{(n)}(I)] \tag{14}$$

IV. The Proposed Algorithm

The dark channel described in (3) can be expressed regarding a morphological erosion as:

$$I^{dark}(\chi) = \left[\varepsilon_S\left(\min_{C\in R,G,B}\left(I^C(y)\right)\right)\right](\chi) \tag{15}$$

Based on (15), a morphological method that can yield an image without haze or halos is proposed as depicted in Fig. 3, and it is described as follows:

Considering $I(\chi)$ as an RGB image of height h and width w pixels, where every pixel position is given by $\chi = (x, y)$, the dark channel $I^{dark}(\chi)$ is computed from $I(\chi)$ according to (15), with the atmospheric light A given by

$$A = \max \sum_{C=1}^{3} I^C \left(\arg\max_{\chi\in(0.1\%*h*w)}\left(I^{dark}(\chi)\right)\right) \tag{16}$$

The image $I(\chi)$ is normalized concerning the atmospheric light A to obtain dark-channel values between zero and one, as given by

$$I_N(\chi) = \frac{I(\chi)}{A} \tag{17}$$

The minimal channel is defined as:

$$I^{\min}(\chi) = \min_{C\in R,G,B}\left(I_N^C(y)\right) \tag{18}$$

The initial transmission map is computed as:

$$t_1(\chi) = 1 - I^{\min}(\chi) \tag{19}$$

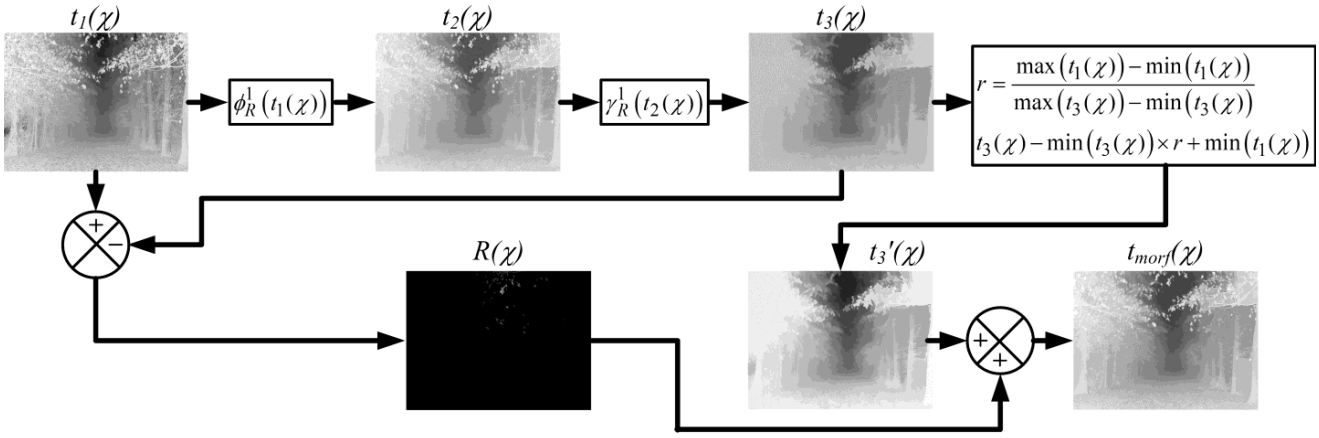

Fig. 4. Morphological process.

Fig. 4 shows each stage of the proposed morphologic process used for refining the initial transmission, which uses a square structuring element S.

In the first stage, a closing by reconstruction is performed as:

$$t_2(\chi) = \phi_R^1(t_1(\chi)) \tag{20}$$

This operation removes small dark elements over the image structuring element.

An opening by reconstruction is carried out later as:

$$t_3(\chi) = \gamma_R^1(t_2(\chi)) \tag{21}$$

This procedure deletes small objects that are clearer than the environment, and its size is smaller than that of S. These objects are saved by

$$R(\chi) = t_1(\chi) - t_3(\chi) \tag{22}$$

To recover the range of values for the original transmission, the intervals of $t_3(\chi)$ are changed to the intervals of $t_1(\chi)$, and the result is saved in $t_3'(\chi)$, as shown by:

$$t_3'(\chi) = t_3(\chi) - \min(t_3(\chi)) \left(\frac{\max(t_1(\chi)) - \min(t_1(\chi))}{\max(t_3(\chi)) - \min(t_3(\chi))} \right) + \min(t_1(\chi)) \tag{23}$$

The refined transmission $t_{morf}(\chi)$ is recovered through:

$$t_{morf}(\chi) = t_3'(\chi) + R(\chi) \tag{24}$$

Fig. 5 shows two examples of transmission maps $t_{morf}(\chi)$ produced by the proposed algorithm.

Finally, the transmission map $t_{morf}(\chi)$ and the atmospheric light A are applied to the scattering model to retrieve the ImageJ(χ) without haze, as shown by

$$J(\chi) = \frac{I(\chi) - A}{t_{morf}(\chi)} + A \tag{25}$$

V. Experimental Results

The proposed algorithm's effectiveness is assessed in this section through experimentation. The obtained results are compared qualitatively and quantitatively against those from different approaches in recent literature. The images used for validating the proposed technique were taken from [28] and [29]. A 15-pixel, square structuring element B was used during the experimentation. The proposed algorithm was implemented on an Intel i5-3320 microprocessor at 2.6 GHz utilizing MATLAB.

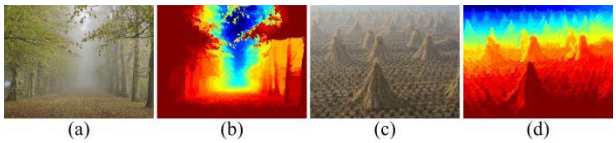

Fig. 5. Examples of transmission maps generated by the proposed algorithm, where (a) (c) are the input images and (b) (d) are the respective transmission maps.

A. Qualitative Comparison

Fig. 6 shows real-world outside images affected by haze that are processed through different state-of-the-art approaches, such as He *et al.* [15] (2017), (c) Tarel *et al.* [18] (2009), (d) Gibson *et al.* [30] (2013), (e) Kim et al [31] (2013), (f) Zhu *et al.* [23] (2015), (g) Berman *et al.* [24] (2016), and the proposed methodology in this work, to carry out a qualitative comparison of the dehazed images obtained through each. He *et al.*'s technique and the proposed method produce an adequate image restoration, qualitatively, since no visible defects are observed. The obtained results from applying Tarel *et al.*'s approach show some artifacts in the restored images (Fig. 6c). The color is visibly affected in the output images (Fig. 6d) from applying Gibson *et al.*'s technique. The Kim *et al.* and Zhu *et al.* schemes present slight halos in their recovered images (Fig. 6e and Fig. 6f, respectively). Finally, Berman *et al.*'s method generates leaves with nonhomogeneous color in the obtained images (Fig. 6g).

B. Quantitative Comparison

Fig. 7 shows eleven images used for numerical analysis of the proposed method's performance compared to other state-of-the-art approaches in the reviewed literature. These images have different characteristics, and they are contaminated with haze simulated by using the model of atmospheric scattering considering the atmospheric light vector [0.92, 0.95, 1] as in [29]; they are then treated during experimentation

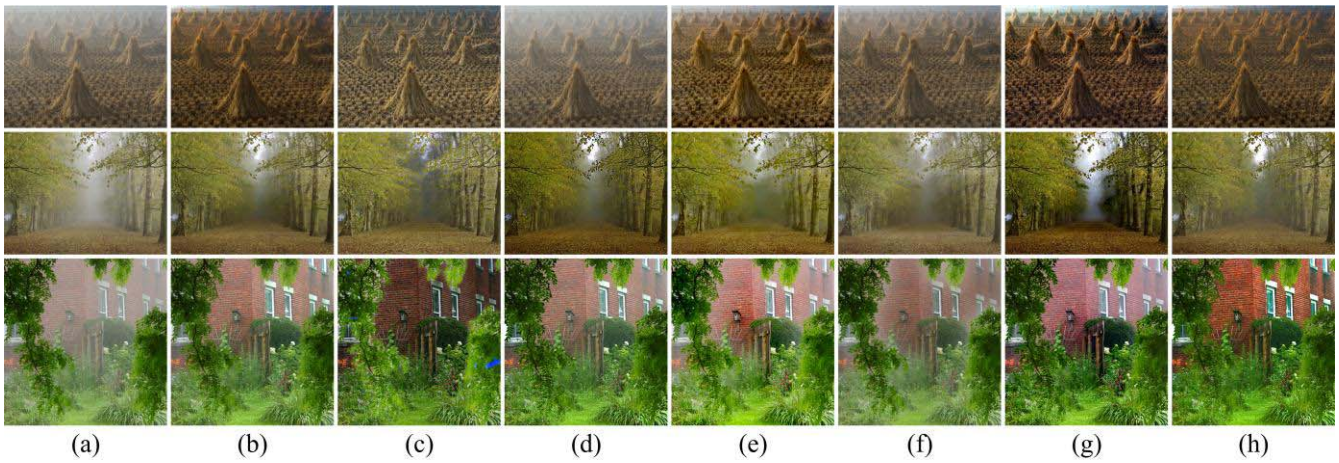

Fig. 6. Comparison of recovered outside real-world scenes without haze. (a) Input images, the results from (b) He *et al.* [15], (c) Tarel *et al.* [18], (d) Gibson *et al.* [30], (e) Kim et al [31], (f) Zhu *et al.* [23], (g) Berman *et al.* [24], and (h) proposed algorithm.

TABLE I
OBTAINED RESULTS FROM PSNR ANALYSIS

Images	He et al. [15]	Tarel et al. [18]	Gibson et al. [30]	Kim et al. [31]	Zhu et al. [23]	Berman et al. [24]	Proposed algorithm
Bikes1	20.7	8.3	15.5	16.2	12.7	26.1	**17.4**
Roofs2	12.9	11.8	14.0	19.2	13.8	16.0	**14.3**
Trees2	18.9	16.1	17.4	15.0	18.9	18.5	**18.0**
Church	19.1	17.2	17.8	18.7	17.2	16.6	**18.4**
Couch	19.9	15.9	20.8	19.1	18.8	12.3	**19.1**
Dolls	18.7	16.9	18.6	19.1	21.1	11.9	**18.8**
Flower1	20.1	16.5	17.0	18.9	18.0	17.4	**19.4**
Flower2	14.8	14.1	15.4	18.2	18.5	15.1	**14.7**
Mansion	18.7	16.0	19.1	17.7	20.5	18.2	**18.7**
Moebius	21.9	11.6	17.5	13.0	15.4	21.0	**20.8**
Raindeer	19.6	10.7	16.6	12.0	13.3	20.8	**18.3**
Average	**18.7**	**14.1**	**17.3**	**17.0**	**17.1**	**17.6**	**18.0**

with the algorithms of He *et al.* [15], Tarel *et al.* [18], Gibson *et al.* [30], Kim *et al.* [31], Zhu *et al.* [23], and Berman *et al.* [24], as well as the approach proposed in this work.

The metrics used for quantitatively evaluating the proposed algorithm's performance against that of previous approaches in the reviewed literature are the peak signal-to-noise ratio (PSNR) and the structural similarity (SSIM) index (27) [32].

PSNR is the proportion between the maximum-possible power of an image and the power of corrupting noise that affects the fidelity of its representation. Given a haze-free image $I_{HF}(\chi)$ and the corresponding mean square error (MSE) between $I_{HF}(\chi)$ and its restored approximation $J(\chi)$, the PSNR is defined by

$$PSNR = 10\log_{10}\left[\frac{MAX^2_{I_{HF}(\chi)}}{MSE}\right] \tag{26}$$

where $MAX^2_{I_{HF}(\chi)}$ is the squared maximum-possible pixel value of the image $I_{HF}(\chi)$, and the corresponding MSE is given as:

$$\text{MSE} = \frac{1}{(w \times h)}\sum_{x=1}^{w}\sum_{y=1}^{h}(J(\chi) - I_{HF}(\chi))^2 \tag{27}$$

with χ representing the pixel position *(x, y)* in the image, with width and height w and h, respectively. The higher the PSNR value, the better the image approximation $J(\chi)$.

The SSIM index is used to measure the similarity between two images, and it considers three aspects in restored images: lighting $l(\chi)$, contrast $c(\chi)$, and structure $s(\chi)$.

$$SSIM(\chi) = f\left(l(\chi), c(\chi), s(\chi)\right) \tag{28}$$

The SSIM index is a decimal value between -1 and 1. SSIM $= 1$ only when two images with identical sets of data are compared.

Fig. 7. Comparison of recovered scenes without haze. (a) Ground-truth images, (b) input images, the results from (c) He *et al.* [15], (d) Tarel *et al.* [18], (e) Gibson *et al.* [30], (f) Kim *et al.* [31], (g) Zhu *et al.* [23], (h) Berman *et al.* [24], and (i) the proposed algorithm.

Table I and Table II show the PSNR and SSIM index metrics, respectively, obtained from each applied approach, and they quantitatively demonstrate the performance superiority of the proposed technique against previously introduced approaches for image dehazing restoration.

C. Time Performance Analysis

Table III presents a time-consumption comparison of the proposed method against state-of-the-art algorithms in the reviewed literature. This table includes information regarding the treated image's size in pixels. A 2.6-GHz, 64-bit Intel Core i5-3320 with 12 GB of RAM was used under the Windows 10 operating system to implement the algorithms in MATLAB 2018a. From this table, it is worth noting that the proposed approach achieves faster processing time than any other technique in the reviewed literature, from one up to four orders of magnitude. In this regard, it is important to point out that, although the approach in He *et al.* [15] obtains higher restoration metrics (PSNR and SSIM), the method introduced in this work is at least three orders of magnitude faster than it. Alternately, the restoration obtained from the introduced technique is quantitatively superior (PSNR y SSIM) and at least one order of magnitude faster than the image restoration from all remaining approaches in the reviewed literature.

Table IV presents a peak memory-consumption comparison of the proposed algorithm against those same approaches in Table III. From Table IV, it is worth noting that the proposed approach has lower memory utilization than all the other considered techniques, except that from Gibson *et al.* [30], for some cases. However, the proposed method surpasses that from Gibson *et al.* with regard to image reconstruction performance and time consumption by at least one order of magnitude.

TABLE II
OBTAINED RESULTS FROM SSIM ANALYSIS

Images	He et al. [15]	Tarel et al. [18]	Gibson et al. [30]	Kim et al. [31]	Zhu et al. [23]	Berman et al. [24]	Proposed algorithm
Bikes1	0.762	0.494	0.644	0.586	0.515	0.848	**0.696**
Roofs2	0.805	0.763	0.853	0.886	0.822	0.883	**0.864**
Trees2	0.866	0.795	0.818	0.571	0.829	0.862	**0.838**
Church	0.833	0.774	0.803	0.815	0.826	0.803	**0.801**
Couch	0.874	0.827	0.919	0.842	0.945	0.707	**0.832**
Dolls	0.879	0.802	0.864	0.820	0.964	0.665	**0.846**
Flower1	0.914	0.843	0.842	0.834	0.876	0.870	**0.893**
Flower2	0.806	0.774	0.832	0.811	0.939	0.830	**0.796**
Mansion	0.837	0.762	0.848	0.716	0.849	0.800	**0.836**
Moebius	0.856	0.655	0.781	0.731	0.662	0.860	**0.820**
Raindeer	0.732	0.546	0.676	0.538	0.579	0.739	**0.703**
Average	**0.833**	**0.731**	**0.807**	**0.741**	**0.801**	**0.806**	**0.811**

TABLE III
COMPUTATIONAL TIME ANALYSIS (SECONDS).

	Image Size (pixels)			
Method	600×400	800×600	1280×720	1920×1080
He et al. [15]	23.35	47.76	97.10	420.98
Tarel et al. [18]	8.13	24.96	111.64	520.02
Gibson et al. [30]	1.19	2.35	4.57	10.43
Kim et al. [31]	0.2	0.3	0.7	1.6
Zhu et al. [23]	0,74	1,31	2,48	5,55
Berman et al. [24]	1,24	2,46	5,12	12,58
Proposed algorithm	**0.02**	**0.04**	**0.06**	**0.14**

TABLE IV
MEMORY UTILIZATION (MEGABYTES)

	Image Size (pixels)			
Method	600×400	800×600	1280×720	1920×1080
He et al. [15]	895.5	1792.5	3472.9	8079.9
Tarel et al. [18]	40.3	82.3	159.7	358.7
Gibson et al. [30]	9.3	18.4	70.3	101.2
Kim et al. [31]	53.3	116.3	215.4	468.7
Zhu et al. [23]	16.6	33.1	63.6	142.7
Berman et al. [24]	117.2	234.5	449.9	1012.5
Proposed algorithm	**13.0**	**23.1**	**43.6**	**90.3**

VI. CONCLUSION

Outdoor images are exposed to adverse weather conditions such as haze, which reduces the visibility of details in a captured scene. Hence, several research works have focused on diminishing haze effects in images by designing and applying dehazing algorithms. In this regard, most of the recently proposed algorithms combine DCP with different techniques that look for fast computation of accurate transmission maps, aiming to preserve the image quality at the cost of long computation times. Therefore, in this work, a novel fast algorithm for lessening haze effects using DCP and a newly introduced approach was compared qualitatively and quantitatively against state-of-the-art techniques; morphological reconstruction is utilized to preserve important structures of the image in all stages. The reviewed literature about the subject involves image reconstruction performance (utilizing PSNR and SSIM index), computation time and memory utilization. From the obtained results, the performance superiority of the proposed method for diminishing haze effects during image reconstruction is clear, as is its high-speed processing time that surpasses all other techniques in the reviewed literature from one to four orders of magnitude with less memory utilization. Therefore, the proposed methodology for image dehazing introduced in this work offers a fast, high-performance dehazing technique suitable for online vision system applications.

Future work will be directed to improve the proposed algorithm's performance in handling sky regions due to DCP limitations.

REFERENCES

[1] C. Chengtao, Z. Qiuyu, and L. Yanhua, "A survey of image dehazing approaches," in *Proc. Control Decis. Conf. (CCDC)*, Qingdao, China, 2015, pp. 3964–3969.
[2] F. Yuan and H. Huang, "Image haze removal via reference retrieval and scene prior," *IEEE Trans. Image Process.*, vol. 27, no. 9, pp. 4395–4409, Sep. 2018.
[3] B. Li *et al.*, "Benchmarking single-image dehazing and beyond," *IEEE Trans. Image Process.*, vol. 28, no. 1, pp. 492–505, Jan. 2019.
[4] K. B. Gibson, D. T. Vo, and T. Q. Nguyen, "An investigation of dehazing effects on image and video coding," *IEEE Trans. Image Process.*, vol. 21, no. 2, pp. 662–673, Feb. 2012.
[5] V. Sahu and M. Singh, "A survey paper on single image dehazing," *Int. J. Recent Innov. Trends Comput. Commun.*, vol. 3, no. 2, pp. 85–88, Feb. 2015.

[6] Y.-H. Lai, Y.-L. Chen, C.-J. Chiou, and C.-T. Hsu, "Single-image dehazing via optimal transmission map under scene priors," *IEEE Trans. Circuit Syst. Video Technol.*, vol. 25, no. 1, pp. 1–14, Jan. 2015.

[7] L. Schaul, C. Fredembach, and S. Süsstrunk, "Color image dehazing using the near-infrared," in *Proc. 16th IEEE Int. Conf. Image Process. (ICIP)*, Cairo, Egypt, Nov. 2009, pp. 1629–1632.

[8] J. Kopf *et al.*, "Deep photo: Model-based photograph enhancement and viewing," *ACM Trans. Graph.*, vol. 27, no. 5, pp. 116-1–116-10, Dec. 2008.

[9] P. Carr and R. Hartley, "Improved single image dehazing using geometry," in *Proc. Digit. Image Comput., Techn. Appl. (DICTA)*, Melbourne, VIC, Australia, 2009, pp. 103–110.

[10] Y. Y. Schechner, S. G. Narasimhan, and S. K. Nayar, "Instant dehazing of images using polarization," in *Proc. IEEE Comput. Soc. Conf. Comput. Vis. Pattern Recognit. (CVPR)*, Kauai, HI, USA, Dec. 2001, pp. I-325–I-332.

[11] Q. Liu, H. Zhang, M. Lin, and Y. Wu, "Research on image dehazing algorithms based on physical model," in *Proc. Int. Conf. Multimedia Technol. (ICMT)*, Hangzhou, China, 2011, pp. 467–470.

[12] X. Wang, X. Jin, G. Xu, and X. Xu, "A multi-scale decomposition based haze removal algorithm," in *Proc. Int. Conf. Remote Sens., Environ. Transp. Eng. (RSETE)*, Nanjing, China, 2012, pp. 1–4.

[13] R. T. Tan, "Visibility in bad weather from a single image," in *Proc. IEEE Conf. Comput. Vis. Pattern Recognit. (CVPR)*, Anchorage, AK, USA, Jun. 2008, pp. 1–8.

[14] R. Fattal, "Single image dehazing," in *Proc. ACM SIGGRAPH ACM Trans. Graph. (TOG)*, vol. 27, no. 3, Aug. 2008, pp. 72:1–72:9.

[15] L. He, J. Zhao, N. Zheng, and D. Bi, "Haze removal using the difference-structure-preservation prior," *IEEE Trans. Image Process.*, vol. 26, no. 3, pp. 1063–1075, Mar. 2017.

[16] K. He, J. Sun, and X. Tang, "Single image haze removal using dark channel prior," *IEEE Trans. Pattern Anal. Mach. Intell.*, vol. 33, no. 12, pp. 2341–2353, Dec. 2011.

[17] W. Wang, F. Chang, T. Ji, and X. Wu, "A fast single-image dehazing method based on a physical model and gray projection," *IEEE Access*, vol. 6, pp. 5641–5653, 2018, doi: 10.1109/ACCESS.2018.2794340.

[18] J.-P. Tarel and N. Hautière, "Fast visibility restoration from a single color or gray level image," in *Proc. 12th IEEE Int. Conf. Comput. Vis. (ICCV)*, Kyoto, Japan, Sep./Oct. 2009, pp. 2201–2208.

[19] N. Gundawar and V. B. Baru, "Improved single image dehazing by fusion," *Int. J. Res. Eng. Technol.*, vol. 3, no. 5, pp. 432–437, May 2014.

[20] R. He, Z. Wang, H. Xiong, and D. D. Feng, "Single image dehazing with white balance correction and image decomposition," in *Proc. Int. Conf. Digit. Image Comput. Techn. Appl. (DICTA)*, Fremantle, WA, Australia, 2012, pp. 1–7.

[21] X. Zhu, Y. Li, and Y. Qiao, "Fast single image dehazing through edge-guided interpolated filter," in *Proc. 14th Int. Conf. Mach. Vis. Appl. (MVA)*, Tokyo, Japan, 2015, pp. 443–446.

[22] J. M. Guo, J.-Y. Syue, V. R. Radzicki, and H. Lee, "An efficient fusion-based defogging," *IEEE Trans. Image Process.*, vol. 26, no. 9, pp. 4217–4228, Sep. 2017.

[23] Q. Zhu, J. Mai, and L. Shao, "A fast single image haze removal algorithm using color attenuation prior," *IEEE Trans. Image Process.*, vol. 24, no. 11, pp. 3522–3533, Nov. 2015.

[24] D. Berman, T. Treibitz, and S. Avidan, "Non-local image dehazing," in *Proc. IEEE Conf. Comput. Vis. Pattern Recognit. (CVPR)*, Las Vegas, NV, USA, Jun. 2016, pp. 1674–1682.

[25] T. M. Bui and W. Kim, "Single image dehazing using color ellipsoid prior," *IEEE Trans. Image Process.*, vol. 27, no. 2, pp. 999–1009, Feb. 2018.

[26] H. Zhang, Q. Liu, F. Yang, and Y. Wu, "Single image dehazing combining physics model based and non-physics model based methods," *J. Comput. Inf. Syst.*, vol. 9, no. 4, pp. 1623–1631, Feb. 2013.

[27] P. Soille, *Morphological Image Analysis: Principles and Applications*, 2nd ed. New York, NY, USA: Springer-Verlag, 2004.

[28] M. Sulami, I. Glatzer, R. Fattal, and M. Werman, "Automatic recovery of the atmospheric light in hazy images," in *Proc. IEEE Int. Conf. Comput. Photogr. (ICCP)*, Santa Clara, CA, USA, May 2014, pp. 1–11.

[29] R. Fattal, "Dehazing using color-lines," *ACM Trans. Graph.*, vol. 34, no. 1, Nov. 2014, Art. no. 13.

[30] K. B. Gibson and T. Q. Nguyen, "Fast single image fog removal using the adaptive wiener filter," in *Proc. IEEE Int. Conf. Image Process. (ICIP)*, Melbourne, VIC, Australia, Sep. 2013, pp. 714–718.

[31] J.-H. Kim, W.-D. Jang, J.-Y. Sim, and C.-S. Kim, "Optimized contrast enhancement for real-time image and video dehazing," *J. Vis. Commun. Image Represent.*, vol. 24, no. 3, pp. 410–425, Apr. 2013.

[32] W. Wang, W. Li, Q. Wang, and M. Qi, "Multiscale single image dehazing based on adaptive wavelet fusion," *Math. Problems Eng.*, vol. 2015, 2015, Art. no. 131082, doi: 10.1155/2015/131082.

Sebastian Salazar-Colores received the B.S. degree in computer science from the Universidad Autónoma Benito Juárez de Oaxaca and the M.S. degree in electrical engineering from the University of Guanajuato. He is currently pursuing the Ph.D. degree with the Universidad Autónoma de Querétaro. His research interests include image processing and computer vision.

Eduardo Cabal-Yepez (M'09) received the M.Eng. degree from the Facultad de Ingenieria Mecanica Electrica y Electronica, Universidad de Guanajuato, Mexico, in 2001, and the Ph.D. degree from the University of Sussex, U.K., in 2007. In 2008, he joined the Division de Ingenierias del Campus Irapuato-Salamanca de la Universidad de Guanajuato, where he is currently a Titular Professor. He is also a National Researcher with the Consejo Nacional de Ciencia y Tecnologia, Mexico. He has authored more than 50 papers in international journals and conferences. His current research interests are digital image and signal processing, artificial intelligence, robotics, smart sensors, real-time processing, mechatronics, FPGAs, and embedded systems.

Juan M. Ramos-Arreguin (SM'17) received the M.S. degree in electrical engineering option instrumentation and digital systems from the University of Guanajuato and the Ph.D. degree in mechatronics science from the Centro de Ingeniería y Desarrollo Industrial. Since 2009, he has been with the Informatics Department, Universidad Autónoma de Querétaro, where he works as a Researcher and a Lecturer. His research interests include mechatronics and embedded systems.

Guillermo Botella received the M.A.Sc. degree in physics, the M.A.Sc. degree in electronic engineering, and the Ph.D. degree from the University of Granada, Spain, in 1998, 2001, and 2007, respectively. He was a Research Fellow funded by EU working with the Department of Architecture and Computer Technology, Universidad de Granada, Spain, and also with the Vision Research Laboratory, University College London, U.K. After that, he joined as an Assistant Professor the Department of Computer Architecture and Automation, Universidad Complutense de Madrid, Spain. He was a Visiting Professor with the Department of Electrical and Computer Engineering, Florida State University, Tallahassee, USA, from 2008 to 2012. He has authored more than 60 papers in international journals and conferences. His current research interests include digital signal processing for very large scale integration (VLSI), FPGAs, vision algorithms, and IP protection of VLSI- and FPGA-based systems. He serves regularly as a reviewer for several IEEE journals.

Luis M. Ledesma-Carrillo (S'13) received the M.Eng. and Ph.D. degrees (Hons.) from the University of Guanajuato, Mexico, in 2013 and 2017, respectively. In 2017, he joined the Division de Ingenierias del Campus Irapuato-Salamanca de la Universidad de Guanajuato, where he is currently an Associate Professor. His fields of interest include digital signal and image processing on field-programmable gate arrays for applications in robotic vision and optics.

Sergio Ledesma (M'13) received the M.S. degree from the University of Guanajuato, while working on the Setup of Internet in Mexico and the Ph.D. degree from the Stevens Institute of Technology, Hoboken, NJ, USA, in 2001. After graduating, he worked for Barclays Global Investors, USA, as part of the IT–HR Group. He has worked as a software engineer for several years. He is currently the Creator of the Software Neural Lab and Wintempla. He is also a Research Professor with the Universidad de Guanajuato, Mexico. His areas of interests are artificial intelligence and software engineering.